AFRL-RX-WP-JA-2017-0192

BOUND FLAVIN−CYTOCHROME MODEL OF EXTRACELLULAR ELECTRON TRANSFER IN SHEWANELLA ONEIDENSIS: ANALYSIS BY FREE ENERGY MOLECULAR (POSTPRINT)

Gongyi Hong and Ruth Pachter

AFRL/RX

23 June 2016
Interim Report

(STINFO COPY)

AIR FORCE RESEARCH LABORATORY
MATERIALS AND MANUFACTURING DIRECTORATE
WRIGHT-PATTERSON AIR FORCE BASE, OH 45433-7750
AIR FORCE MATERIEL COMMAND
UNITED STATES AIR FORCE

REPORT DOCUMENTATION PAGE

Form Approved
OMB No. 0704-0188

1. REPORT DATE (DD-MM-YY)	2. REPORT TYPE	3. DATES COVERED (From - To)
23 June 2016	Interim	11 January 2013- 10 October 2015

4. TITLE AND SUBTITLE	5a. CONTRACT NUMBER
BOUND FLAVIN−CYTOCHROME MODEL OF EXTRACELLULAR ELECTRON TRANSFER IN SHEWANELLA ONEIDENSIS: ANALYSIS BY FREE ENERGY MOLECULAR (POSTPRINT)	FA8650-09-D-5430-0025
	5b. GRANT NUMBER
	5c. PROGRAM ELEMENT NUMBER 62102F

6. AUTHOR(S)	5d. PROJECT NUMBER
Gongyi Hong and Ruth Pachter – AFRL/RX	4348
	5e. TASK NUMBER
	5f. WORK UNIT NUMBER X0KU

7. PERFORMING ORGANIZATION NAME(S) AND ADDRESS(ES)	8. PERFORMING ORGANIZATION REPORT NUMBER
AFRL/RX Wright-Patterson AFB, OH 45433	

9. SPONSORING/MONITORING AGENCY NAME(S) AND ADDRESS(ES)	10. SPONSORING/MONITORING AGENCY ACRONYM(S)
Air Force Research Laboratory Materials and Manufacturing Directorate Wright-Patterson Air Force Base, OH 45433-7750 Air Force Materiel Command United States Air Force	AFRL/RXAP
	11. SPONSORING/MONITORING AGENCY REPORT NUMBER(S) AFRL-RX-WP-JA-2017-0192

12. DISTRIBUTION/AVAILABILITY STATEMENT
Distribution Statement A. Approved for public release: distribution unlimited.

13. SUPPLEMENTARY NOTES

14. ABSTRACT *(Maximum 200 words)*
Flavins are known to enhance extracellular electron transfer (EET) in Shewanella oneidensis MR-1 bacteria, which reduce electron acceptors through outer-membrane (OM) cytochromes c. Free-shuttle and bound-redox cofactor mechanisms were proposed to explain this enhancement, but recent electrochemical reports favor a flavin-bound model, proposing two one-electron reductions of flavin, namely, oxidized (Ox) to semiquinone (Sq) and semiquinone to hydroquinone (Hq), at anodic and cathodic conditions, respectively. In this work, to provide a mechanistic understanding of riboflavin (RF) binding at the multiheme OM cytochrome OmcA, we explored binding configurations at hemes 2, 5, 7, and 10. Subsequently, on the basis of molecular dynamics (MD) simulations, binding free energies and redox potential shifts upon RF binding for the Ox/Sq and Sq/Hq reductions were analyzed. Our results demonstrated an upshift in the Ox/Sq and a downshift in the Sq/Hq redox potentials, consistent with a bound RF−OmcA model. Furthermore, binding free energy MD simulations indicated an RF binding preference at heme 7

15. SUBJECT TERMS
Flavin; extracellular electron transfer (EET); Shewanella oneidensis MR-1 bacteria; outer-membrane (OM) cytochromes

| 16. SECURITY CLASSIFICATION OF:			17. LIMITATION OF ABSTRACT:	18. NUMBER OF PAGES	19a. NAME OF RESPONSIBLE PERSON (Monitor)
a. REPORT Unclassified	**b. ABSTRACT** Unclassified	**c. THIS PAGE** Unclassified	SAR	10	Ruth Pachter **19b. TELEPHONE NUMBER** (Include Area Code) (937) 255-9689

Bound Flavin–Cytochrome Model of Extracellular Electron Transfer in *Shewanella oneidensis*: Analysis by Free Energy Molecular Dynamics Simulations

Gongyi Hong and Ruth Pachter*

Air Force Research Laboratory, Materials and Manufacturing Directorate, Wright-Patterson Air Force Base, Ohio 45433, United States

ⓢ *Supporting Information*

ABSTRACT: Flavins are known to enhance extracellular electron transfer (EET) in *Shewanella oneidensis* MR-1 bacteria, which reduce electron acceptors through outer-membrane (OM) cytochromes *c*. Free-shuttle and bound-redox cofactor mechanisms were proposed to explain this enhancement, but recent electrochemical reports favor a flavin-bound model, proposing two one-electron reductions of flavin, namely, oxidized (Ox) to semiquinone (Sq) and semiquinone to hydroquinone (Hq), at anodic and cathodic conditions, respectively. In this work, to provide a mechanistic understanding of riboflavin (RF) binding at the multiheme OM cytochrome OmcA, we explored binding configurations at hemes 2, 5, 7, and 10. Subsequently, on the basis of molecular dynamics (MD) simulations, binding free energies and redox potential shifts upon RF binding for the Ox/Sq and Sq/Hq reductions were analyzed. Our results demonstrated an upshift in the Ox/Sq and a downshift in the Sq/Hq redox potentials, consistent with a bound RF−OmcA model. Furthermore, binding free energy MD simulations indicated an RF binding preference at heme 7. MD simulations of the OmcA−MtrC complex interfacing at hemes 5 revealed a small interprotein redox potential difference with an electron transfer rate of 10^7-10^8/s.
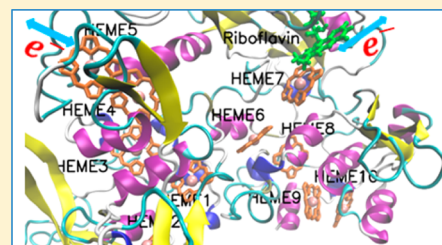
I. INTRODUCTION

Microbial nanowires have attracted great interest recently, for example, for bioenergy,[1] including for use in microbial fuel cells,[2] catalysis,[3] reduction of graphene oxide to mitigate use of toxic chemicals,[4] protection of steel from corrosion,[5] or in bioremediation.[6] Of special interest is the potential use of the exoelectrogens in neurophysiology nanoelectronics.[7] Indeed, it was pointed out that exoelectrogens are a critical part of microbial electrochemical technologies that aim to impact applications in biosensing and biocomputing.[8] For example, Leung et al.[9] have shown that *Shewanella oneidensis* MR-1 exoelectrogens exhibit p-type, tunable electronic behavior with mobility comparable to that of organic semiconductors. Interestingly, the adsorption and electron transfer on the gold surface of the deca-heme cytochrome MtrF was recently investigated.[10] At the same time, the extracellular electron transfer (EET) for the anaerobic respiration process in *S. oneidensis* MR-1 that can use multiple electron acceptors, including solid minerals, was extensively investigated,[11] where reduction of electron acceptors requires electron transfer across the outer membrane (OM). The so-called "electron conduit" is comprised of multiheme *c*-type cytochromes, and electrons generated in the cell are transferred toward the extracellular anode. This biological conduit can also transport electrons into cells under cathodic conditions.[12]

El-Naggar and co-workers[13,14] proposed that the electron transport occurs through multistep hopping along chains of hemes in MtrCAB−OmcA complexes.[15] MtrC and OmcA are deca-heme cytochromes located at the OM exterior surface.[15,16]

MtrB is an OM β-barrel porin comprising 28 transmembrane β-strands, and MtrA is a deca-heme periplasmic protein which associates with the OM at the interior surface.[15] MtrF, MtrD, and MtrE are homologues of MtrC, MtrA, and MtrB.[16] MtrC(F) transfer electrons directly to an extracellular electron acceptor or indirectly through other OM cytochromes such as OmcA.[14,17] The multiheme OM cytochromes are organized into four clades, and crystal structures were determined by Clarke and co-workers for MtrF,[16] UndA,[18] OmcA,[19] and MtrC.[20] The hemes in the OM cytochromes are arranged as a staggered cross with hemes 2 and 7, 5, and 10 located in the opposite ends of shorter and longer crossbeams, respectively, as shown in Figure 1.

Recently, Okamoto et al. demonstrated that bound cell-secreted flavin redox cofactors enhance EET,[12,21−23] namely, riboflavin (RF) and flavin mononucleotide (FMN), which specifically associate with OmcA and MtrC, respectively, while a free-form model of soluble flavin shuttles was discussed by Marsili et al.[24] NMR spectroscopy provided evidence that interactions between the redox cofactors with OmcA and MtrC occur near the hemes.[25] This process can provide ways to enhance EET, such as in modulating the ionic strength to strengthen the RF redox cofactor binding affinity,[26] or through development of a synthetic flavin biosynthesis pathway from *Bacillus subtilis* expressed in *S. oneidensis*.[27] El-Naggar and co-
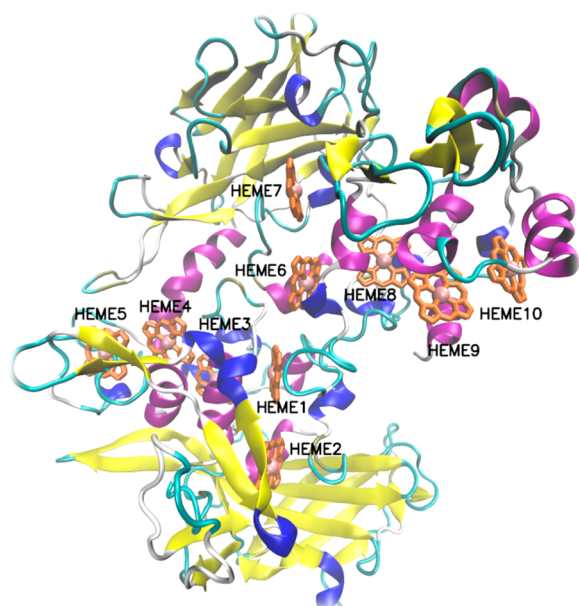
Figure 1. Arrangement of hemes in the OmcA OM cytochrome.[19]

workers also investigated the role of the electrode type in discerning EET of free- and bound-flavin models of *S. oneidensis* MR-1.[28] Two distinct peaks in the differential pulse voltammetry measurements were observed, corresponding to both free and cytochrome-bound flavin models, due to the use of a carbon cloth electrode.[28]

An electrochemical study[12] has shown that, under anodic conditions, a one-electron reduction of the oxidized RF (Ox) to semiquinone (Sq) is involved in the EET (eq 1), with the corresponding redox potential (E^0) measured as −110 mV (against SHE), where

$$RF(Ox) + e^- + H^+ \rightarrow RFH^\bullet(Sq) \qquad (1)$$

Under cathodic conditions, the one-electron reduction of RF Sq to hydroquinone (Hq) (eq 2) has a measured E^0 of −400 mV, where

$$RFH^\bullet(Sq) + e^- \rightarrow RFH^-(Hq) \qquad (2)$$
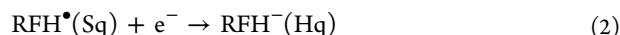
For free RF in aqueous solution, E^0 of −314 mV[29] was measured for the Ox/Sq reaction, while the one-electron Sq/Hq reduction has a redox potential of −124 mV.[29] Therefore, for bound RF−OmcA under anodic conditions, the Ox/Sq redox potential was upshifted by 204 mV.[12] At the cell−cathode interface, E^0 of Sq/Hq was downshifted by 276 mV. A relative negative redox potential of the Sq/Hq redox reaction for bound RF−OmcA results in thermodynamically unfavorable electron flow back from the heme to the cathode.[12]

However, despite these recent developments, details of the RF-bound system were not examined, and a crystal structure of the complex is not available. To provide an atomic-level understanding of the RF-bound OmcA model and demonstrate consistency with experimental electrochemical data, we report an investigation of RF-bound OmcA complexes based on free energy molecular dynamics (MD) simulations. Following molecular docking of the RF redox cofactor at OmcA heme sites, which were derived from the crystal structure,[19] binding free energies were analyzed. Changes in binding free energies by mutation of hydrophobic residues at binding sites were also considered. On the basis of the RF−OmcA bound systems,

redox potential shifts were calculated by MD simulations and the predicted trends were found to be consistent with experiment. Modeling of the complexation of OmcA and MtrC demonstrated that the interprotein electron transfer rate is comparable to those among hemes in MtrF.

II. COMPUTATIONAL METHODS

II.1. Docking. Docking of RF was carried out with AutoDock Vina,[30] where a semiempirical free energy force field was used,[31] which scores binding of a small molecule to protein sites, including pairwise atomic terms for repulsion and London dispersion, hydrogen bonding, electrostatics, and desolvation. The exhaustiveness parameter used was set higher than the default value to ensure a better search. Polar hydrogens were added, and Kollman[32] charges were used for the protein, where the calculated electrostatic potential is fit to the partial charge model. The input was prepared with the MGL tools http://mgltools.scripps.edu/downloads/mgltools-1-5-6-release-candidate%20tools.[33] The OmcA X-ray structure (pdb: 4LMH)[19] was kept rigid, but all rotatable bonds in RF were included.

II.2. MD Simulations. Simulations were performed with GROMACS version 5.0.x,[34] using the AMBER03 force field for the protein.[35] The general AMBER force field[36] (GAFF) was used for RF and for dihedral angle terms of the hemes. Force constants for bonding and angular terms for hemes were derived from the Hessian of the optimized geometry of a model compound,[37,38] as shown in Figure S1 in the Supporting Information. The model system includes two His ligands (modeled as methyl-imidazole) and heme B with its covalently linked two Cys residues (CH_3CH_2S) through two thioether bonds formed between the heme porphyrin atoms CAB and CAC (labeled in Figure S2a) with the Cys S atom. The geometry of the complex was optimized at the DFT M06[39]/6-31G* level (the singlet Fe(II) state for heme was adopted as the strong ligand field, since the bis-imidazole coordination renders the ferric and ferrous hemes to be in low-spin states[16]). Force constants are listed in Table S1. RESP[32] charges for RF and hemes with ligated His and bonded Cys residues were obtained by B3LYP/6-31G* calculations, followed by analysis with AmberTools 14.[40]

MD simulations at constant NPT for 10 ns were then performed. Particle-mesh Ewald sums[41] were applied for efficient treatment of long-range electrostatics with a short-range cutoff of 1 nm and a relative strength of the electrostatic interaction at the cutoff of 10^{-5} at 1 nm (spacing of 0.12 nm, interpolation order of 6). A 1.2 nm cutoff was used in calculating the Lennard-Jones potential. The LINCS algorithm was chosen to reset bonds to their correct lengths after an unconstrained update.[42] The temperature was regulated by velocity rescaling with a stochastic term of 0.1 ps, and the pressure by the Berendsen weak coupling method. The protein was solvated in a box of water with a distance of 1 nm separating the solute and the box wall.

II.3. Free Energy Calculations. To calculate the free energy change of two different end states, an alchemical path[43] was used to connect them. Stratification or multistate sampling was applied to reduce the systematic error, in which a sequence of intermediate states are introduced for the two end states (U_A and U_B), such that $U(\lambda) = (1 - \lambda)U_A + \lambda U_B$ and $\Delta G = G_1 - G_0 = \sum_{i=0}^{n-1}[G_{\lambda_{i+1}} - G_{\lambda_i}]$. To avoid numerical singularity problems in the decoupling procedure, a soft-core potential was intro-
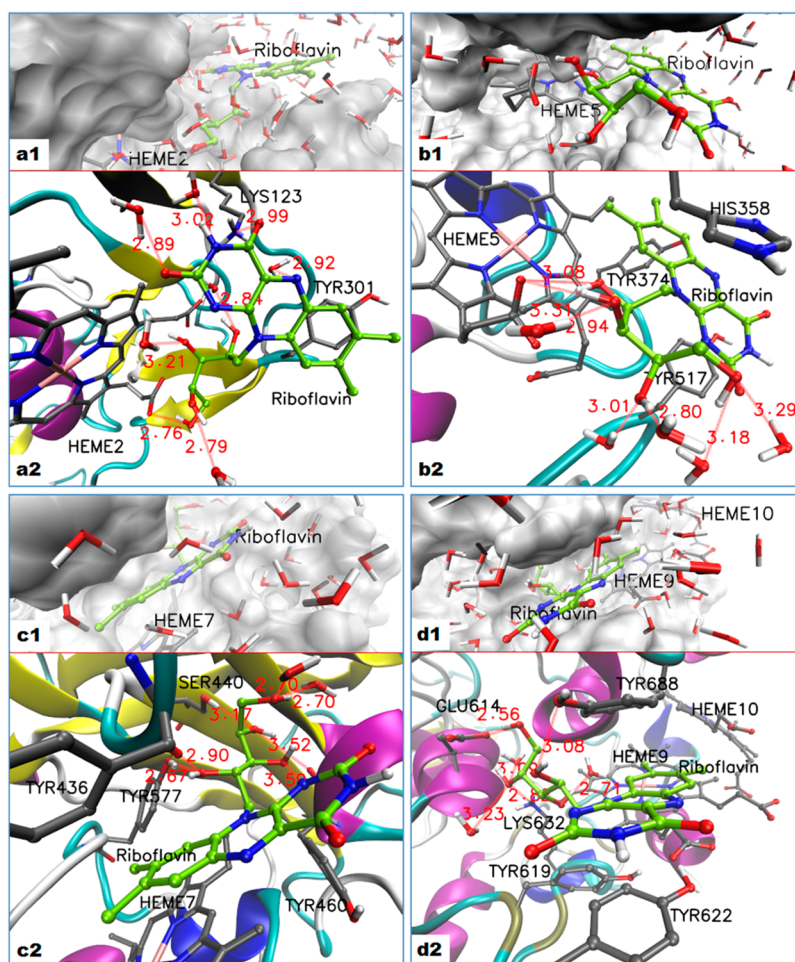
Figure 2. Binding pockets and hydrogen bonding of RF near hemes 2 (a1, a2), 5 (b1, b2), 7 (c1, c2), and 10 (d1, d2). Proximate residues and hydrogen bond distances (red, in Å) are shown.

duced,[44] where $V_{AB}^{sc}(r) = (1 - \lambda)V_A(R_A(r, \lambda)) + \lambda V_B(R_B(r, \lambda))$, with $R_A(r, \lambda) = (\alpha\sigma_A{}^6\lambda^p + r^6)^{1/6}$ and $R_B(r, \lambda) = (\alpha\sigma_A{}^6(1 - \lambda)^p + r^6)^{1/6}$, and V_A and V_B are van der Waals (vdW) potentials for states A and B, respectively, and the soft-core potential recovers the A state for $\lambda = 0$ and the B state for $\lambda = 1$. In practical calculations, $p = 1$, $\alpha = 0.5$, and $\sigma = 0.3$. For each window (λ_i), the following procedure was applied: (1) geometry optimization; (2) equilibration at constant NVT for 100 ps; (3) equilibration at constant NPT for 100 ps; (4) MD simulation (sampling) at constant NPT for 1 ns. For the decoupling protocol in binding free energy calculations, 5 ns MD simulations were carried out both for NPT equilibration and for sampling to ensure sufficient sampling. As λ changes from 0 to 1 (see Table S2), the Bennett acceptance ratio method[45] implemented in GROMACS was used to calculate the free energy difference between different states. For each window λ_i, the potential energy difference in both the forward $\Delta U_{i,k}^f = U_{i+1}(x_{i,k}) - U_i(x_{i,k})$ and reverse $\Delta U_{i,k}^r = U_{i+1}(x_{i+1,k}) - U_i(x_{i+1,k})$ directions was sampled. The free energy difference ΔA between window i and $i + 1$ was computed by solving

$$\sum_{k=1}^{n_i} \frac{1}{1 + \frac{n_i}{n_j}\exp[(\Delta U_{i,k}^f - \Delta A)/k_B T]} =$$

$$\sum_{k=1}^{n_j} \frac{1}{1 + \frac{n_j}{n_i}\exp[(\Delta A - \Delta U_{i,k}^r)/k_B T]}$$

where $n_i(n_j)$ are the number of sampling configurations at window $i(i + 1)$.

In binding free energy calculations, the virtual bond algorithm[46] was followed to confine RF in the binding pocket of OmcA, using six geometrical parameters, where $(r_0, \theta_0, \varphi_0)$ are the distance, angle, and dihedral angle that describe the position of the ligand relative to the protein, and $(\alpha_0, \beta_0, \gamma_0)$ are the angles and dihedral angles that describe its orientation (defined in Figure S2a). The translational so-called restraint potential in polar coordinates implemented in GROMACS is given by $u(r, \theta, \varphi) = \frac{1}{2}K_r(r - r_0)^2 + K_\theta(1 - \cos(\theta - \theta_0)) + \frac{1}{2}K_\varphi(\varphi - \varphi_0)^2$, and the rotational restraint potential by $u(\alpha, \beta, \gamma) = K_\alpha(1 - \cos(\alpha - \alpha_0)) + \frac{1}{2}K_\beta(\beta - \beta_0)^2 + \frac{1}{2}K_\gamma(\gamma - \gamma_0)^2$. For a given binding molecule (L), the configurational partition function can be written as $Z_L = Z_L^{ext} \times Z_L^{int}$, where Z_L^{ext} arises from translational and rotational external degrees of freedom (DOFs) and Z_L^{int} from internal DOFs. $Z_L^{ext} = 8\pi^2 V$ for a nonlinear molecule. For one molar standard state, V equals 1660 Å^3. After applying the restraint potential to the molecule $(L^\ddagger)$, we have $Z_{L^\ddagger} = Z_{L^\ddagger}^{ext} \times Z_{L^\ddagger}^{int}$, such that $Z_{L^\ddagger}^{ext} = \int_0^\infty r^2 \, dr \int_0^\pi \sin\theta \, d\theta \int_{-\pi}^\pi d\varphi e^{-u(r,\theta,\varphi)/kT} \int_0^\pi \sin\alpha \, d\alpha \int_{-\pi}^\pi d\beta \int_{-\pi}^\pi d\gamma e^{-u(\alpha,\beta,\gamma)/kT}$. Here T is the temperature and k is the Boltzmann constant. Since there are no cross interaction terms among the six external DOFs, their contribution to the partition function can be calculated separately with numerical integration methods such as Simpson's rule.[47]

III. RESULTS AND DISCUSSION

III.1. Binding Free Energies. In MtrF, the binding site of a soluble substrate was proposed to be near hemes 2 or 7,[16] in UndA near heme 7,[18] and for OmcA, the dimer structure was reported to interface at hemes 5, while heme 10 was assumed the electron egress site.[19] A molecular docking study of FMN binding at MtrC hemes found overall weak binding with a slight preference for heme 2,[48] while a similar investigation for anthraquinone-2,6-disulfonate docking at UndA hemes has shown preference for hemes 2 and 7.[25] We considered RF binding at hydrophobic pockets of OmcA near hemes 2, 5, 7, and 10. Following identification of hydrophobic pockets in the OmcA X-ray structure,[19] molecular docking calculations were performed. Subsequently, starting from the docked RF bound OmcA structures with strongest binding affinity, all-atom MD simulations with explicit solvent were carried out. The resulting RF−OmcA structures are shown in Figure 2, indicating hydrogen bonding and hydrophobic residues at the binding sites.

Examination of the binding sites demonstrates that, for RF bound near hemes 5, 7, and 10, the flavin isoalloxazine ring is almost parallel to the heme porphyrin plane, and the nonpolar ring (1,2-dimethylbenzene ring, see RF structure in Figure S2b) approaches the heme, while the polar ring with the −NH and −CO groups reaches out. For RF near heme 2, the isoalloxazine ring is approximately perpendicular to the heme porphyrin plane. RF's polar side is close to the heme, with the −NH and one −CO groups forming H-bonds with nearby water molecules, and one −CO group forming an H-bond with Lys123. The nonpolar part of RF is also exposed to the solvent. For hemes 5, 7, and 10, the flavin isoalloxazine ring is partially inserted within the binding pocket, which involves His358, Tyr374, and Tyr517 for heme 5, Tyr436, and heme's porphyrin for heme 7, and Tyr688, Tyr622, and heme 9's porphyrin for heme 10. For heme 2, the flavin ring stacks against the Tyr301 phenol ring. In all cases, one or more Tyr residues are involved in the binding pocket, as is known for flavoproteins, where aromatic stacking between the flavin isoalloxazine ring and hydrophobic residues, such as Tyr and Trp, plays a major role in the binding process.[49] The ribityl −OH groups (2'-OH, 3'-OH, 4'-OH, and 5'-OH in Figure S2b) form hydrogen bonds with the protein or solvent water molecules. For heme 2, 2'-OH, 3'-OH, and 4'-OH form hydrogen bonds with a nearby water molecule, while 5'-OH with heme 2's porphyrin acetate group. For heme 5, 4'-OH and 5'-OH form hydrogen bonds with a nearby water molecule, while 2'-OH and 3'-OH with heme 2's porphyrin acetate group. For heme 7, 2'-OH forms a hydrogen bond with the Tyr577 −OH group and the backbone −CO group, 3'-OH with the N1 atom, and 4'-OH with Ser440's −OH group and the backbone −CO group of Tyr460, and 5'-OH with a nearby water molecule. For heme 10, 2'-OH forms a hydrogen bond with −OH of Tyr688, 3'-OH with a nearby water molecule, and 4'-OH with Lys632 and 5'-OH with the Glu614 acetate group.

Binding free energies of oxidized RF near hemes 2, 5, 7, and 10 in OmcA were calculated by the alchemical double decoupling method[43,44] with a restraint potential, as illustrated in Figure 3. The binding free energy (ΔG_b^0) of RF to OmcA in aqueous solution is described by $(OmcA)_{H_2O} + (RF)_{H_2O} \xrightarrow{\Delta G_b^0}$ $(OmcA - RF)_{H_2O}$.[46] Following common practice, the interaction between RF and the environment for both free
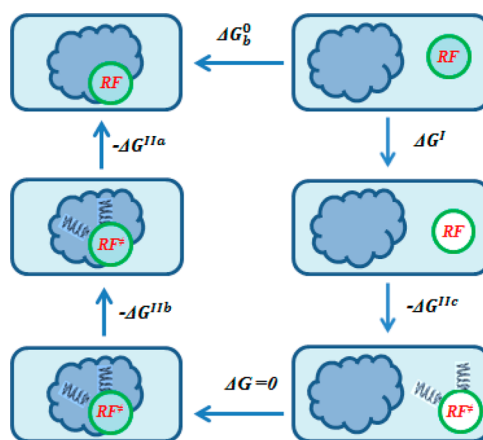
Figure 3. Thermodynamic cycle used to calculate the RF binding free energy at OmcA hemes. ΔG^I denotes the free energy change upon turning off the interaction between free RF and water; ΔG^{IIa} is the free energy change after exerting a restraint potential to confine the position and orientation of bound RF; ΔG^{IIb} is the free energy change when decoupling the interaction between restrained bound RF (RF‡) and the environment; ΔG^{IIc} denotes the free energy change of removing the external restraint potential.

RF in solution and RF bound at OmcA were decoupled, such that $(RF)_{H_2O} \xrightarrow{\Delta G^I} (RF)_{vac}$ and $(OmcA - RF)_{H_2O} \xrightarrow{\Delta G^{II}}$ $(OmcA)_{H_2O} + (RF)_{vac}$, and $\Delta G_b^0 = \Delta G^I - \Delta G^{II}$. A restraint potential was applied to confine bound RF's position and orientation and avoid its wandering when interaction with the environment was turned off,[43] so that $(OmcA - RF)_{H_2O} \xrightarrow{\Delta G^{IIa}}$ $(OmcA - RF^‡)_{H_2O} \xrightarrow{\Delta G^{IIb}} (OmcA)_{H_2O} + (RF^‡)_{vac} \xrightarrow{\Delta G^{IIc}}$ $(OmcA)_{H_2O} + (RF)_{vac}$. $\Delta G_b^0 = \Delta G^I - \Delta G^{IIa} - \Delta G^{IIb} - \Delta G^{IIc}$, where ‡ denotes a restrained state. ΔG^I, ΔG^{IIa}, and ΔG^{IIb} were readily calculated by free energy MD simulations using the alchemical path and the free energy change of switching off the restraint potential by $\Delta G^{IIc} = -kT \ln\left(\frac{8\pi^2 V}{Z_{L^‡}^{ext}}\right)$ (see Computational Methods).

Calculated binding free energies of RF bound at wild-type (WT) and site-mutated OmcA with all heme groups reduced are listed in Table 1. RF bound near hemes 5 and 7 has a relatively stronger affinity, with binding free energies of −35.7 and −38.2 kJ/mol, respectively, while the binding affinity near hemes 2 and 10 is relatively weaker, with binding free energies of −20.7 and −22.6 kJ/mol, respectively, smaller by about 15 kJ/mol. Interestingly, the binding affinity of RF near heme 7 was −20.5 kJ/mol when all heme groups were oxidized, decreasing by about 18 kJ/mol compared to the respective system with reduced hemes. Note that bound redox flavin cofactors were only observed for reduced MtrC.[23]

In examining contributions of electrostatic and vdW interactions to the binding affinity, we note that the relatively weaker binding at hemes 2 and 10 is mainly due to a smaller contribution of vdW interactions because the isoalloxazine ring of RF at heme 2 is exposed to the solvent, leaving only Tyr301 for aromatic stacking. For heme 10, the RF isoalloxazine ring is loosely stacked with neighboring hydrophobic residues, while weaker binding of RF at heme 7 for oxidized OmcA is due to a weaker electrostatic interaction. In exploring details of binding

Table 1. Binding Free Energies (kJ/mol) with OmcA Hemes in the Reduced State[a]

binding site	ΔG^{I}	$-\Delta G^{IIa}$	$-\Delta G^{IIb}$			$-\Delta G^{IIc}$	ΔG_b^0
			electrostatic	vdW	total		
2(WT)	106.04	−19.31	−110.88	−35.61	−146.49	39.10	−20.66
5(WT)	106.04	−12.12	−95.60	−74.45	−170.05	40.45	−35.68
7(WT)	106.04	−8.66	−106.74	−68.52	−175.26	39.69	−38.19
7(WT)[b]	106.04	−14.97	−79.9	−72.15	−152.05	40.49	−20.49
7(A436)	106.04	−8.59	−99.05	−53.29	−152.34	39.12	−15.77
7(W436)	106.04	−10.94	−94.82	−65.01	−159.83	39.98	−24.75
10(WT)	106.04	−8.47	−108.29	−51.37	−159.66	39.46	−22.63
10(A688)	106.04	−7.77	−112.31	−50.85	−163.16	39.97	−24.92
10(W688)	106.04	−12.20	−107.77	−57.63	−165.40	39.50	−32.06

[a]A description of the free energy terms is given in the text. [b]Hemes in oxidized state.

upon mutation, we found that Tyr436/Ala436 and Tyr436/Trp436 mutations within the binding pocket near heme 7 decreased the binding affinity by 22.4 and 13.4 kJ/mol, respectively, as expected. On the other hand, Trp688/Ala688 and Tyr688/Trp688 mutations increased the binding affinity for the binding pocket near heme 10 by ca. 2.3 and 9.4 kJ/mol, respectively. To assess the sensitivity of the binding affinity to the details of the binding site, alternative binding sites at hemes 2, 5, 7, and 10 were explored (see description and Figure S3 in the Supporting Information), resulting in binding energies comparable to those reported here.

III.2. Redox Potential Shifts. Next, we calculated the redox potential shift of RF bound at OmcA compared to free RF in solution. First, on the basis of the thermodynamic cycle shown in Figure 4, redox reaction 1 was considered. The difference in
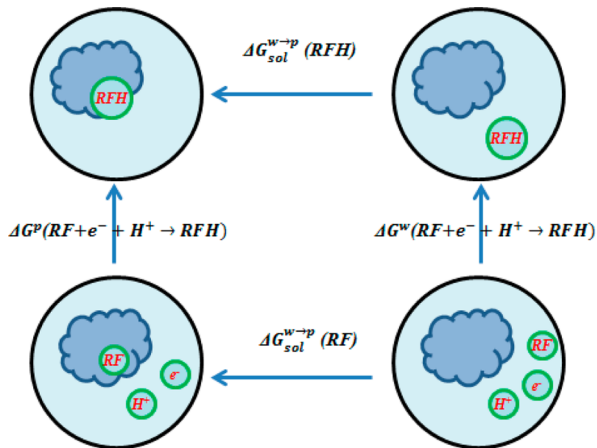

Figure 4. Thermodynamic cycle used to calculate the redox potential shift when moving the RF redox cofactor from water to the OmcA protein for the one-electron reduction reaction Ox/Sq.

the Ox/Sq reaction free energy can be derived from the free energy difference between Ox(RF) and Sq(RFH) in protein and in water, where

$$\Delta\Delta G = \Delta G^{w \to p}(RF + e^- + H^+ \to RFH)$$
$$= \Delta G_{sol}^p(RF \to RFH) - \Delta G_{sol}^w(RF \to RFH) \quad (3)$$

To calculate the solvation free energy difference of RFH and RF (RFH has an extra hydrogen bonded to the N5 atom, as compared to RF; see the structure of RF in Figure S2b), we designed reference states RFH0 and RF0, which have the same

molecular structure as RFH and RF, respectively, but no electrostatic interaction with the environment, so that

$$\Delta G_{sol}^{p(w)}(RF \to RFH)$$
$$= \Delta G_{sol}^{p(w)}(RF \to RF0) + \Delta G_{sol}^{p(w)}(RF0 \to RFH0)$$
$$+ \Delta G_{sol}^{p(w)}(RFH0 \to RFH)$$
$$= \Delta G_{sol}^{p(w)}(RF \to RF0) - \Delta G_{sol}^{p(w)}(RFH \to RFH0)$$
$$- \Delta G_{sol}^{p(w)}(RFH0 \to RF0) \quad (4)$$

Specifically, to change RF to RF0 or RFH to RFH0, the electrostatic interaction between RF and the environment is decoupled, while, from RFH0 to RF0, the vdW interaction between H(N5) and the environment is decoupled, which is negligible in our calculations.

Next, we considered reaction 2. The redox potential shift when moving RF from solution to OmcA for the Sq/Hq redox reaction is related to the free energy difference

$$\Delta\Delta G = \Delta G^p(RFH + e^- \to RFH^-)$$
$$- \Delta G^w(RFH + e^- \to RFH^-) \quad (5)$$

In practice, an additional free RFH was placed and restrained around 2.5 nm away from the protein surface. The free energy change upon electron transfer from free RFH⁻ in the solvent to RFH bound at OmcA was calculated using an alchemical path, in which state A corresponds to RFH⁻(free) + RFH(bound) and state B corresponds to RFH(free) + RFH⁻(bound). The redox potential shift for eqs 3 and 5 is given by

$$\varepsilon_p^0 - \varepsilon_w^0 = -\frac{\Delta\Delta G}{F} = -\Delta\Delta G \times 10.4 \quad (6)$$

where the redox potential is in mV and $\Delta\Delta G$ in kJ/mol. Since the redox potentials for the Ox/Sq and Sq/Hq reactions were measured under anodic and cathodic conditions, oxidized and reduced heme states were assumed, respectively.

The calculated results are summarized in Table 2. The solvation free energies for RF and RFH are similar in water yet demonstrate significant changes in the bound state, attributed to differences in atomic partial charge distributions within the protein environment. An upshift of the Ox/Sq reduction potential of bound RF vs free RF was indeed reproduced, although the calculated values of 58, 58, 101, and 59 mV for binding sites near hemes 2, 5, 7, and 10 are smaller than the experimentally derived estimate of 204 mV. The downshifts of the one-electron Sq/Hq for binding sites near hemes 2, 5, 7, and 10 were calculated as −105, −240, −469, and −498 mV,

Table 2. Free Energy Differences (kJ/mol) for Reactions 1 and 2^a

	heme 2	heme 5	heme 7	heme 10	Exp.[12]
Ox/Sq (eq 1)					
$\Delta G_{sol}^{p}(RF \rightarrow RFH)$	−5.3	−5.3	−9.4	−5.4	
$\Delta G_{sol}^{w}(RF \rightarrow RFH)$	0.3	0.3	0.3	0.3	
$\Delta G_{sol}^{p}(RF \rightarrow RFH) - \Delta G_{sol}^{w}(RF \rightarrow RFH)$	−5.6	−5.6	−9.7	−5.7	
$\varepsilon_{p}^{0} - \varepsilon_{w}^{0}$	58	58	101	59	204
Sq/Hq (eq 2)					
$\Delta G^{p}(RFH + e^{-} \rightarrow RFH^{-1}) - \Delta G^{w}(RFH + e^{-} \rightarrow RFH^{-1})$	10.2	23.2	45.3	48.0	
$\varepsilon_{p}^{0} - \varepsilon_{w}^{0}$	−105	−240	−469	−497	−276

$^a\varepsilon_{p}^{0} - \varepsilon_{w}^{0}$ is the shift in reduction potentials for the Ox/Sq and Sq/Hq redox reactions when RF changes from free-form in solution to bound at OmcA (mV).

respectively, while the experimental value is −276 mV. Encouragingly, the trend in redox potentials is predicted correctly, while a quantitative comparison to experiment for this complex electrochemical system is beyond the scope of current methodologies and available experimental data. For example, the measured potential of the two-electron free-form molecular flavin reduction of −240 mV[28] is larger than the value of −207 mV measured without the cellular context.[50]

III.3. Electron Transfer between MtrC and OmcA. To further understand EET in this case, complexation of OmcA and MtrC with hemes 5 at the interface was investigated. Edwards et al.[19] pointed out that heme 5 shows the largest variation among crystal structures, suggesting that this could be the site of electron exchange. In addition, it was demonstrated[19] that the OmcA crystal structure and oligomeric structure in solution are in excellent agreement. OmcA and MtrC[20] were first docked with ZDOCK,[51] followed by a MD simulation for 100 ns at constant NPT ($T = 300$ K), in which only heme 5 of OmcA is in the reduced state and all other 19 hemes are in the oxidized state. The resulting complex is shown in Figure 5,
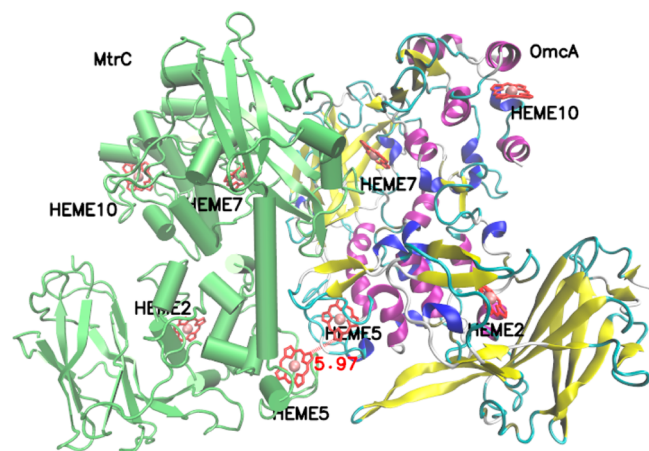
Figure 5. Complex of OmcA and MtrC. The distance between hemes 5 is given in Å.

revealing shape compensation at the interface between OmcA and MtrC upon binding, and a close contact in the region around hemes 7 and heme 5 with an edge-to-edge distance between the porphyrins of hemes 5 of 5.97 Å. This is consistent with a value of 5.97 Å calculated for the MtrF−OmcA complex,[52] but our MtrC−OmcA complex exhibits a more

compact structure. The rate of electron transfer (k_{ET}) based on Marcus theory[53] is given by $\log(k_{ET}) = 15 - 0.434\beta R - 3.1[(\Delta G + \lambda)^2/\lambda]$, where ΔG and λ are the Gibbs free energy and reorganization energy (eV), respectively. A β value of 1.4 Å^{-1} is often assumed,[54] intermediate between doped semiconductors and a vacuum,[55] and R is the edge−edge distance between two heavy atoms in hemes.

Free energy MD simulations to examine electron transfer from OmcA's heme 5 to MtrC's heme 5 were performed using an alchemical path, where states A and B designate Fe(II)$_{Heme5,OmcA}$, Fe(III)$_{Heme5,MtrC}$ and Fe(III)$_{Heme5,OmcA}$, Fe(II)$_{Heme5,MtrC}$, respectively. The reorganization energy was calculated using the linear response approximation[56] by $\lambda = 0.5(\langle V_B - V_A \rangle_A - \langle V_B - V_A \rangle_B)$, where V_A (V_B) are potential energies when the active site is in state A (B), calculated by MD simulations. The sampling procedure is similar to the reaction free energy calculation except that only the initial and final states are involved without intermediate states. A small reaction free energy of about 99 mV and reorganization energy of 1.1 eV were calculated. Calculated uphill and downhill electron transfer rates (k_{ET}) were 2.3×10^7 and 3.9×10^8/s, respectively, comparable to the electron transfer rate between intrahemes in MtrF.[57] Note that *in vivo* OmcA forms a complex with MtrC at the end of the MtrABC complex and not with free MtrC.

IV. CONCLUSION

In this work, we investigated binding affinity and changes in the redox properties of riboflavin upon binding to OmcA near hemes 2, 5, 7, and 10. Molecular docking combined with MD simulation refinement and subsequent MD free energy calculations were performed, where derivation of force field parameters for the hemes was carried out. The calculated reduction potential was upshifted for the Ox/Sq redox reaction as compared to free RF in solution, favoring withdrawal of electrons from the cell, and downshifted for the Sq/Hq redox reaction, consistent with experimental measurements. Binding free energies demonstrated a binding preference of RF at hemes 5 and 7. However, heme 5 may interface with other proteins, thus leaving heme 7 as a likely binding site, where the binding affinity was also sensitive to Y436/A436 mutation. Although heme 7 is relatively insulated inside the protein, the bound riboflavin cofactor extends toward the surface. This observation could prompt experimental investigation of mutated OmcA to assess the role of heme 7. MD simulations for the OmcA and MtrC complex with interfacing hemes 5

6

resulted in a relatively small edge-to-edge distance and a small redox potential difference, with k_{ET} comparable to that between intraprotein hemes.

■ ASSOCIATED CONTENT

Ⓢ Supporting Information

The Supporting Information is available free of charge on the ACS Publications website at DOI: 10.1021/acs.jpcb.6b03851.

> Model compound used for heme force constant calculations and listing of force constants, decoupling parameters, heme–RF system description, and alternative binding configurations of RF near hemes 2, 5, 7, and 10 (PDF)

■ AUTHOR INFORMATION

Corresponding Author

*E-mail: ruth.pachter@us.af.mil. Phone: (937) 255-9689.

Notes

The authors declare no competing financial interest.

■ ACKNOWLEDGMENTS

■ REFERENCES

(1) Malvankar, N. S.; Lovley, D. R. Microbial Nanowires for Bioenergy Applications. *Curr. Opin. Biotechnol.* **2014**, *27*, 88−95.

(2) Logan, B. E. Exoelectrogenic Bacteria that Power Microbial Fuel Cells. *Nat. Rev. Microbiol.* **2009**, *7*, 375−381.

(3) Bewley, K. D.; Ellis, K. E.; Firer-Sherwood, M. A.; Elliott, S. J. Multi-Heme Proteins: Nature's Electronic Multi-Purpose Tool. *Biochim. Biophys. Acta, Bioenerg.* **2013**, *1827*, 938−948.

(4) Jiao, Y.; Qian, F.; Li, Y.; Wang, G.; Saltikov, C. W.; Gralnick, J. A. Deciphering the Electron Transport Pathway for Graphene Oxide Reduction by Shewanella oneidensis MR-1. *J. Bacteriol.* **2011**, *193*, 3662−3665.

(5) Dubiel, M.; Hsu, C. H.; Chien, C. C.; Mansfeld, F.; Newman, D. K. Microbial Iron Respiration can Protect Steel from Corrosion. *Appl. Environ. Microbiol.* **2002**, *68*, 1440−1445.

(6) Williams, K. H.; Bargar, J. R.; Lloyd, J. R.; Lovley, D. R. Bioremediation of Uranium-Contaminated Groundwater: A Systems Approach to Subsurface Biogeochemistry. *Curr. Opin. Biotechnol.* **2013**, *24*, 489−497.

(7) Angle, M. R.; Cui, B.; Melosh, N. A. Nanotechnology and Neurophysiology. *Curr. Opin. Neurobiol.* **2015**, *32*, 132−140.

(8) Ter Avest, M. A.; Ajo-Franklin, C. M. Transforming Exoelectrogens for Biotechnology Using Synthetic Biology. *Biotechnol. Bioeng.* **2016**, *113*, 687−697.

(9) Leung, K. M.; Wanger, G.; El-Naggar, M. Y.; Gorby, Y.; Southam, G.; Lau, W. M.; Yang, J. Shewanella oneidensis MR-1 Bacterial Nanowires Exhibit p-Type, Tunable Electronic Behavior. *Nano Lett.* **2013**, *13*, 2407−2411.

(10) Wei, T.; Ma, H.; Nakano, A. Decaheme Cytochrome MtrF Adsorption and Electron Transfer on Gold Surface. *J. Phys. Chem. Lett.* **2016**, *7*, 929−936.

(11) Breuer, M.; Rosso, K. M.; Blumberger, J.; Butt, J. N. Multi-Haem Cytochromes in Shewanella oneidensis MR-1: Structures, Functions and Opportunities. *J. R. Soc., Interface* **2015**, *12*, 1−27.

(12) Okamoto, A.; Hashimoto, K.; Nealson, K. H. Flavin Redox Bifurcation as a Mechanism for Controlling the Direction of Electron Flow During Extracellular Electron Transfer. *Angew. Chem., Int. Ed.* **2014**, *53*, 10988−10991.

(13) Pirbadian, S.; El-Naggar, M. Y. Multistep Hopping and Extracellular Charge Transfer in Microbial Redox Chains. *Phys. Chem. Chem. Phys.* **2012**, *14*, 13802−13808.

(14) Pirbadian, S.; Barchinger, S. E.; Leung, K. M.; Byun, H. S.; Jangir, Y.; Bouhenni, R. A.; Reed, S. B.; Romine, M. F.; Saffarini, D. A.; Shi, L.; et al. Shewanella oneidensis MR-1 Nanowires are Outer Membrane and Periplasmic Extensions of the Extracellular Electron Transport Components. *Proc. Natl. Acad. Sci. U. S. A.* **2014**, *111*, 12883−12888.

(15) Hartshorne, R. S.; Reardon, C. L.; Ross, D.; Nuester, J.; Clarke, T. A.; Gates, A. J.; Mills, P. C.; Fredrickson, J. K.; Zachara, J. M.; Shi, L.; et al. Characterization of an Electron Conduit Between Bacteria and the Extracellular Environment. *Proc. Natl. Acad. Sci. U. S. A.* **2009**, *106*, 22169−22174.

(16) Clarke, T. A.; Edwards, M. J.; Gates, A. J.; Hall, A.; White, G. F.; Bradley, J.; Reardon, C. L.; Shi, L.; Beliaev, A. S.; Marshall, M. J.; et al. Structure of a Bacterial Cell Surface Decaheme Electron Conduit. *Proc. Natl. Acad. Sci. U. S. A.* **2011**, *108*, 9384−9389.

(17) Shi, L.; Rosso, K. M.; Clarke, T. A.; Richardson, D. J.; Zachara, J. M.; Fredrickson, J. K. Molecular Underpinnings of Fe(III) Oxide Reduction by Shewanella oneidensis MR-1. *Front. Microbiol.* **2012**, *3*, 50.

(18) Edwards, M. J.; Hall, A.; Shi, L.; Fredrickson, J. K.; Zachara, J. M.; Butt, J. N.; Richardson, D. J.; Clarke, T. A. The Crystal Structure of the Extracellular 11-heme Cytochrome UndA Reveals a Conserved 10-heme Motif and Defined Binding Site for Soluble Iron Chelates. *Structure (Oxford, U. K.)* **2012**, *20*, 1275−1284.

(19) Edwards, M. J.; Baiden, N. A.; Johs, A.; Tomanicek, S. J.; Liang, L.; Shi, L.; Fredrickson, J. K.; Zachara, J. M.; Gates, A. J.; Butt, J. N.; Richardson, D. J.; Clarke, T. A. The X-Ray Crystal Structure of Shewanella oneidensis OmcA Reveals New Insight at the Microbe-Mineral Interface. *FEBS Lett.* **2014**, *588*, 1886−1890.

(20) Edwards, M. J.; White, G. F.; Norman, M.; Tome-Fernandez, A.; Ainsworth, E.; Butt, J. N.; Richardson, D. J.; Clarke, T. A.; Shi, L.; Fredrickson, J. K.; Zachara, J. M. Redox Linked Flavin Sites in Extracellular Decaheme Proteins Involved in Microbe-Mineral Electron Transfer. *Sci. Rep.* **2015**, *5*, 11677.

(21) Okamoto, A.; Nakamura, R.; Nealson, K. H.; Hashimoto, K. Bound Flavin Model Suggests Similar Electron-Transfer Mechanisms in Shewanella and Geobacter. *ChemElectroChem* **2014**, *1*, 1808−1812.

(22) Okamoto, A.; Kalathil, S.; Deng, X.; Hashimoto, K.; Nakamura, R.; Nealson, K. H. Cell-Secreted Flavins Bound to Membrane Cytochromes Dictate Electron Transfer Reactions to Surfaces with Diverse Charge and pH. *Sci. Rep.* **2014**, *4*, 5628.

(23) Okamoto, A.; Hashimoto, K.; Nealson, K. H.; Nakamura, R. Rate Enhancement of Bacterial Extracellular Electron Transport Involves Bound Flavin Semiquinones. *Proc. Natl. Acad. Sci. U. S. A.* **2013**, *110*, 7856−7861.

(24) Marsili, E.; Baron, D. B.; Shikhare, I. D.; Coursolle, D.; Gralnick, J. A.; Bond, D. R. Shewanella Secretes Flavins that Mediate Extracellular Electron Transfer. *Proc. Natl. Acad. Sci. U. S. A.* **2008**, *105*, 3968−3973.

(25) Paquete, C. M.; Fonseca, B. M.; Cruz, D. R.; Pereira, T. M.; Pacheco, I.; Soares, C. M.; Louro, R. O. Exploring the Molecular Mechanisms of Electron Shuttling Across the Microbe/Metal Space. *Front. Microbiol.* **2014**, *5*, 318.

(26) Kalathil, S.; Hashimoto, K.; Okamoto, A. Effect of Ionic Strength on the Rate of Extracellular Electron Transport in Shewanella oneidensis MR-1 through Bound-Flavin Semiquinones. *ChemElectroChem* **2014**, *1*, 1840−1843.

(27) Yang, Y.; Ding, Y.; Hu, Y.; Cao, B.; Rice, S. A.; Kjelleberg, S.; Song, H. Enhancing Bidirectional Electron Transfer of Shewanella oneidensis by a Synthetic Flavin Pathway. *ACS Synth. Biol.* **2015**, *4*, 815−823.

(28) Xu, S.; Jangir, Y.; El-Naggar, M. Y. Disentangling the Roles of Free and Cytochrome-Bound Flavins in Extracellular Electron Transport from Shewanella oneidensis MR-1. *Electrochim. Acta* **2016**, *198*, 49−55.

(29) Anderson, R. F. Energetics of the One-Electron Reduction Steps of Riboflavin, FMN and FAD to their Fully Reduced Forms. *Biochim. Biophys. Acta, Bioenerg.* **1983**, *722*, 158−162.

(30) Trott, O.; Olson, A. J. AutoDock Vina: Improving the Speed and Accuracy of Docking with a New Scoring Function, Efficient Optimization, and Multithreading. *J. Comput. Chem.* **2010**, *31*, 455−461.

(31) Huey, R.; Morris, G. M.; Olson, A. J.; Goodsell, D. S. A Semiempirical Free Energy Force Field with Charge-Based Desolvation. *J. Comput. Chem.* **2007**, *28*, 1145−1152.

(32) Singh, U. C.; Kollman, P. A. An Approach to Computing Electrostatic Charges for Molecules. *J. Comput. Chem.* **1984**, *5*, 129.

(33) Morris, G. M.; Huey, R.; Lindstrom, W.; Sanner, M. F.; Belew, R. K.; Goodsell, D. S.; Olson, A. J. AutoDock4 and AutoDockTools4: Automated Docking with Selective Receptor Flexibility. *J. Comput. Chem.* **2009**, *30*, 2785−2791.

(34) Hess, B.; Kutzner, C.; van der Spoel, D.; Lindahl, E. GROMACS 4: Algorithms for Highly Efficient, Load-Balanced, and Scalable Molecular Simulation. *J. Chem. Theory Comput.* **2008**, *4*, 435−447.

(35) Duan, Y.; Wu, C.; Chowdhury, S.; Lee, M. C.; Xiong, G.; Zhang, W.; Yang, R.; Cieplak, P.; Luo, R.; Lee, T.; Caldwell, J.; Wang, J.; Kollman, P. A Point-Charge Force Field for Molecular Mechanics Simulations of Proteins Based on Condensed-Phase Quantum Mechanical Calculations. *J. Comput. Chem.* **2003**, *24*, 1999−2012.

(36) Wang, J.; Wolf, R. M.; Caldwell, J. W.; Kollman, P. A.; Case, D. A. Development and Testing of a General Amber Force Field. *J. Comput. Chem.* **2004**, *25*, 1157−1174.

(37) Seminario, J. M. Calculation of Intramolecular Force Fields from Second-Derivative Tensors. *Int. J. Quantum Chem.* **1996**, *60*, 1271−1277.

(38) Nilsson, K.; Lecerof, D.; Sigfridsson, E.; Ryde, U. An Automatic Method to Generate Force-Field Parameters for Hetero-Compounds. *Acta Crystallogr., Sect. D: Biol. Crystallogr.* **2003**, *59*, 274−289.

(39) Zhao, Y.; Truhlar, D. The M06 Suite of Density Functionals for Main Group Thermochemistry, Thermochemical Kinetics, Non-covalent Interactions, Excited States, and Transition Elements: Two New Functionals and Systematic Testing of Four M06-Class Functionals and 12 Other Functionals. *Theor. Chem. Acc.* **2008**, *120*, 215−241.

(40) Case, D. A.; Babin, V.; Berryman, J. T.; Betz, R. M.; Cai, Q.; Cerutti, D. S.; Cheatham, T. E., III; Darden, T. A.; Duke, R. E.; Gohlke, H.; et al. *Ambertools 14*; University of California: San Francisco, CA, 2014.

(41) Essmann, U.; Perera, L.; Berkowitz, M. L.; Darden, T.; Lee, H.; Pedersen, L. G. A Smooth Particle Mesh Ewald Method. *J. Chem. Phys.* **1995**, *103*, 8577−8593.

(42) Hess, B.; Bekker, H.; Berendsen, H. J. C.; Fraaije, J. G. E. M. LINCS: A Linear Constraint Solver for Molecular Simulations. *J. Comput. Chem.* **1997**, *18*, 1463−1472.

(43) Deng, Y.; Roux, B. Computations of Standard Binding Free Energies with Molecular Dynamics Simulations. *J. Phys. Chem. B* **2009**, *113*, 2234−2246.

(44) Pohorille, A.; Jarzynski, C.; Chipot, C. Good Practices in Free-Energy Calculations. *J. Phys. Chem. B* **2010**, *114*, 10235−10253.

(45) Bennett, C. H. Efficient Estimation of Free Energy Differences from Monte Carlo Data. *J. Comput. Phys.* **1976**, *22*, 245−268.

(46) Boresch, S.; Tettinger, F.; Leitgeb, M.; Karplus, M. Absolute Binding Free Energies: A Quantitative Approach for Their Calculation. *J. Phys. Chem. B* **2003**, *107*, 9535−9551.

(47) Deng, Y.; Roux, B. Calculation of Standard Binding Free Energies: Aromatic Molecules in the T4 Lysozyme L99A Mutant. *J. Chem. Theory Comput.* **2006**, *2*, 1255−1273.

(48) Breuer, M.; Rosso, K. M.; Blumberger, J. Flavin Binding to the Deca-heme Cytochrome MtrC: Insights from Computational Molecular Simulation. *Biophys. J.* **2015**, *109*, 2614−2624.

(49) Lostao, A.; Daoudi, F.; Irun, M. P.; Ramon, A.; Fernandez-Cabrera, C.; Romero, A.; Sancho, J. How FMN Binds to Anabaena Apoflavodoxin: A Hydrophobic Encounter at an Open Binding Site. *J. Biol. Chem.* **2003**, *278*, 24053−24061.

(50) Mayhew, S. G. The effects of pH and Semiquinone Formation on the Oxidation-Reduction Potentials of Flavin Mononucleotide. A Reappraisal. *Eur. J. Biochem.* **1999**, *265*, 698−702.

(51) Pierce, B. G.; Wiehe, K.; Hwang, H.; Kim, B.-H.; Vreven, T.; Weng, Z. ZDOCK Server: Interactive Docking Prediction of Protein-Protein Complexes and Symmetric Multimers. *Bioinformatics* **2014**, *30*, 1771−1773.

(52) Nakano, C. M.; Byun, H. S.; Ma, H.; Wei, T.; El-Naggar, M. Y. A Framework for Stochastic Simulations and Visualization of Biological Electron-Transfer Dynamics. *Comput. Phys. Commun.* **2015**, *193*, 1−9.

(53) Marcus, R. A.; Sutin, N. *Biochim. Biophys. Acta, Rev. Bioenerg.* **1985**, *811*, 265.

(54) Moser, C. C.; Keske, J. M.; Warncke, K.; Farid, R. S.; Dutton, P. L. Nature of Biological Electron Transfer. *Nature (London, U. K.)* **1992**, *355*, 796−802.

(55) Edwards, P. P.; Gray, H. B.; Lodge, M. T. J.; Williams, R. J. P. Electron Transfer and Electronic Conduction Through an Intervening Medium. *Angew. Chem., Int. Ed.* **2008**, *47*, 6758−6765.

(56) Sham, Y. Y.; Chu, Z. T.; Tao, H.; Warshel, A. Examining Methods for Calculations of Binding Free Energies: LRA, LIE, PDLD-LRA, and PDLD/S-LRA Calculations of Ligands Binding to an HIV Protease. *Proteins: Struct., Funct., Genet.* **2000**, *39*, 393−407.

(57) Breuer, M.; Rosso, K. M.; Blumberger, J. Electron Flow in Multiheme Bacterial Cytochromes is a Balancing Act between Heme Electronic Interaction and Redox Potentials. *Proc. Natl. Acad. Sci. U. S. A.* **2014**, *111*, 611−616.